Nanoscale

ARTICLE

# Colloidal quantum dot lasers built on a passive two-dimensional photonic crystal backbone

Hojun Chang,[a,b] Kyungtaek Min,[a,b] Myungjae Lee,[a,b] Minsu Kang,[a,b] Yeonsang Park,[c] Kyung-Sang Cho,[c] Young-Geun Roh,[c] Sung Woo Hwang,[c] and Heonsu Jeon*[a,b,d]

We report room-temperature lasing action from two-dimensional photonic crystal (PC) structures composed of a passive Si_3N_4 backbone with CdSe/CdS/ZnS colloidal quantum dots (CQDs) over-coated for optical gain. When optically excited, devices lased at dual PC band-edge modes, with the modal dominance governed by the thickness of CQD over-layer. The demonstrated laser platform should have impact on the future photonic integrated circuits as the on-chip coupling between active and passive components is readily achievable.

Ever since the first demonstration,[1] lasers whose resonance is provided by the principle of *photonic crystal* (PC) have been actively studied because they can be operated in a very small scale in terms of size as well as input energy and therefore have an application potential for the future high-density photonic integrated circuits. Although laser operation within an even smaller cavity can be achieved by utilizing localized surface plasmon resonance (LSPR),[2,3] it suffers from significant optical loss accompanying intrinsically to plasmonic materials; consequently, typical room-temperature laser threshold densities of the LSPR-based nanolasers are abnormally high (on the order of GW/cm^2),[4,5] and therefore can only be operated in pulsed mode, which limits their practicality and applicability. In good contrast, PC-based laser structures are composed of all dielectrics and thus have no intrinsic optical loss, resulting in laser operation under continuous-wave condition with reasonably low lasing thresholds.[6-10] For this reason, PC-based lasers are the only practical device platforms conceivable at the present stage of nanolaser development.

As for optical gain material, conventional PC lasers utilize an epitaxially grown thin-film compound semiconductor containing multiple quantum wells (MQWs). An array of air-holes are perforated into the MQW epilayer to produce a two-dimensional (2D) PC structure with desired photonic band properties; a defect structure may or may not be included, depending on the types of resonance to be used. The PC membrane layer is either suspended in the air or bonded onto an extrinsic low refractive index substrate to satisfy the waveguide condition along the wafer plane. However, this conventional "resonance structure carved out of gain material" approach[1,11] not only wastes much of the valuable epitaxial material, but is also hard to adopt for photonic integrated circuits where active and passive photonic components are to be integrated in high density. Here we demonstrate another class of PC laser that is built under the concept of "gain material applied onto a passive resonance structure". To realize such a laser, we employ colloidal quantum dots (CQDs) as optical gain material. CQDs are advantageous over the epitaxially grown MQWs in many aspects. First of all, monodisperse CQDs can be chemically synthesized[12,13] and therefore highly cost-effective. More importantly, their emission wavelengths can be tailored simply by the physical size of individual CQD without changing the composing materials. Introduction of the core-shell structure boosted
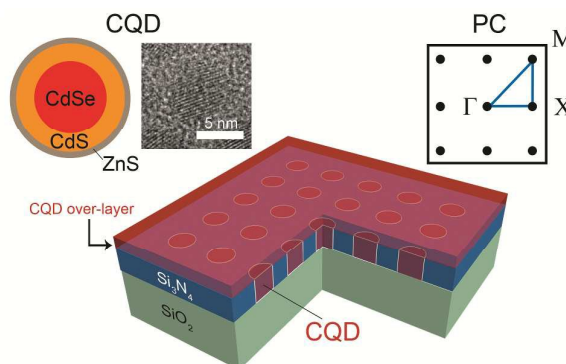
Fig. 1 Schematic of CQD-PC band-edge laser structure. The Si_3N_4 waveguide slab perforated with a square lattice array of air-holes serves a passive PC backbone on SiO_2-cladding/Si-substrate. Spin-coated CQDs not only infiltrate the air-holes but also form a thin over-layer. Shown together are (left) a schematic structure as well as a transmission electron microscope image of the CdSe/CdS/ZnS core-shell-shell CQD and (right) the reciprocal lattice of square lattice PC with high symmetry points marked.

[a] Department of Physics and Astronomy, Seoul National University, Seoul 08826, Republic of Korea
[b] Inter-university Semiconductor Research Center, Seoul National University, Seoul 08826, Republic of Korea
[c] Samsung Advanced Institute of Technology, Suwon 11678, Republic of Korea
[d] Department of Biophysics and Chemical Biology, Seoul National University, Seoul 08826, Republic of Korea
* E-mail: hsjeon@snu.ac.kr
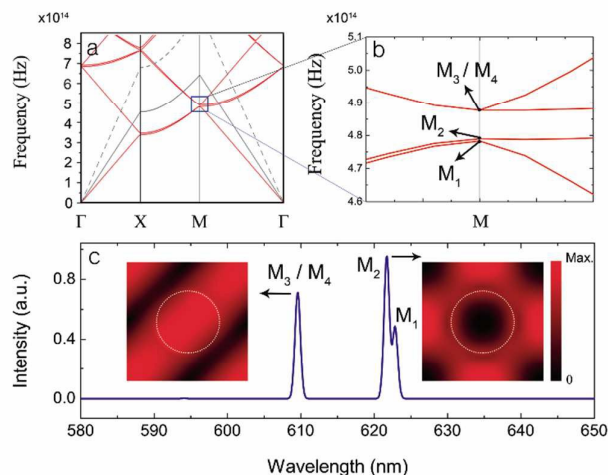
Fig. 2 Photonic band structure and M-point band-edge mode properties of the 2D square lattice CQD-PC structure. (a)(b) Photonic band structure calculated by 3D FDTD: (a) overall and (b) near the M-point band-edges. Also shown in (a) are the light lines in vacuum (gray broken line) and in SiO_2 (gray solid line). (c) Resonant mode spectrum calculated for the M-point band-edges, exhibiting two HIB band-edge modes (M_1 and M_2) at $\lambda \sim 622$ nm and two degenerate LIB band-edge modes (M_3 and M_4) at $\lambda \sim 610$ nm. The insets display the band-edge mode profiles (transverse E-field intensity) for M_2 and M_3/M_4, also calculated by 3D FDTD (the mode profile for M_1 is omitted since it is very similar to that for M_2.).

up the quantum efficiency of CQDs,[14-16] which subsequently resulted in CQD lasing action when incorporated into an appropriate cavity structure, such as vertical-cavity surface-emitting lasers (VCSELs)[17,18] or distributed feed-back (DFB) laser.[19] Therefore, the application of CQDs (for optical gain) to a passive PC structure (for optical resonance) can be a cost-effective way of preparing nanolasers that are not only compact and efficient but also can be integrated with other passive optical components on a single chip. It should be quite appropriate to note some precedent studies on beneficial effects of combining a PC structure with nano-emitters, such as spontaneous emission control[20-25] or efficient energy transfer,[26-28] although they are remote from lasing action.

Our strategy in fabricating CQD-PC lasers is to combine a "top-down" (the formation of a passive PC backbone structure) and a "bottom-up" (the introduction of CQD material) method. To be more specific, we prepare an air-hole based 2D PC slab waveguide composed of a fully passive material to prepare optical resonance via PC band-edge modes, which is followed by the over-coat of highly luminescent CQDs to provide optical gain extrinsically—Fig. 1. Band-edge modes have been one of the major laser resonance mechanism utilized in demonstrating PC lasers.[29-36] Note that CQDs are assumed not only to infiltrate the air-holes but also to form a thin over-layer on top of the entire device, which is inevitable at the present stage as explained later. The waveguide slab is therefore composed of a passive material of high refractive index and a thin CQD over-layer, and is designed such that it supports only a single vertical waveguide mode at CQD emission wavelengths. For laser resonance, we choose the M-point band-edge modes of a 2D square-lattice PC. In order to determine structural parameters of the 2D PC, we have performed computer simulations based on three-

dimensional (3D) finite-difference time-domain (FDTD) method. Figure 2a shows calculated photonic band structure of the designed 2D square-lattice PC for the transverse-electric (TE) polarization. The lattice constant and air-hole diameter of the 2D PC are $a = 255$ nm and $2r = 140$ nm, respectively, while the waveguide structure is assumed to consist of a Si_3N_4 slab ($n_{\_Si3N4} = 2.01$; $t_{\_Si3N4} = 140$ nm) and a CQD over-layer ($n_{\_CQD} = 1.75$; $t_{\_CQD} = 100$ nm), which is sandwiched between the claddings of a fused silica ($n_{\_SiO2} = 1.45$) in the bottom and the air ($n_{\_air} = 1$) in the above. At the M-point which we choose for laser resonance, there are total four band-edge modes: M_1, M_2, M_3, and M_4—Fig. 2b. We may group them in terms of which band the band-edge modes belong to: M_1 and M_2 to the high index band (HIB), and M_3 and M_4 to the low index band (LIB). Figure 2c is a FDTD-simulated mode spectrum, exhibiting all the M-point band-edge modes. Please note that M_3 and M_4 are perfectly degenerate modes in energy so that they merge into one peak in the spectrum. Shown as the insets are the transverse electric field intensity profiles ($E_t^2 \equiv E_x^2 + E_y^2$) of two representative band-edge modes, M_2 and M_3. The mode profiles of M_1 and M_4 are not shown because M_1 is very similar to that of M_2, while M_3 and M_4 are identical except for the mode orientation rotated by 90°. It is worth noting that the modal intensity is concentrated in the dielectric region for M_2 and in the air-hole for M_3, which is consistent with their belongings to the HIB and LIB, respectively.

The CQD-PC band-edge lasers were fabricated as follows. First, a 140-nm-thick Si_3N_4 slab was deposited by plasma-enhanced chemical-vapor deposition (PECVD) on top of a thick SiO_2 cladding layer on Si substrate. A 2D square-lattice hole array was patterned
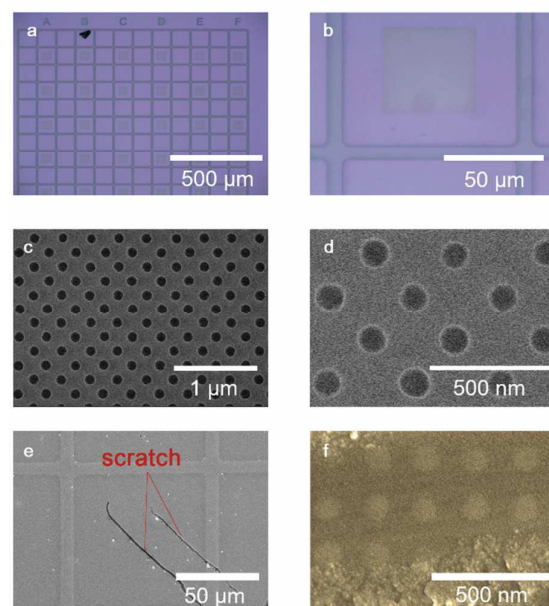
Fig. 3 Images of fabricated CQD-PC laser devices. (a)(b) Optical microscope images of fabricated Si_3N_4 PC backbone with the mesh grid pattern for device identification. (c)(d) SEM images of the fabricated Si_3N_4 PC backbone. (e)(f) SEM images of fully fabricated CQD-PC devices including the spin-coating of CQDs on the Si_3N_4 PC backbone: (e) the

CQD over-layer was scratched intentionally and (f) high-quality CQD filling into the air-holes is confirmed.

by electron-beam lithography. The PC pattern formed on the resist layer was transferred to the underlying Si_3N_4 layer by reactive-ion etching (RIE), resulting in a Si_3N_4 PC slab on top of SiO_2 cladding. In order to facilitate device identification during subsequent optical measurements, a mesh grid trench was generated by conventional microlithography and RIE. Figure 3a shows an optical microscope image taken for the 6 × 6 PC array with the mesh grid in-between, while Fig. 3b is an amplified image of a PC pattern of 50 μm × 50 μm in size. Figure 3c and 3d are scanning electron microscope (SEM) images of the Si_3N_4 PC backbone in two different magnifications, demonstrating the formation of clean and uniform circular air-holes into the Si_3N_4 layer. In order to compensate possible uncertainty in theoretical predictions as well as experimental tolerance, we intentionally varied the nominal air-hole diameter ($2r$ = 120-150 nm); the nominal PC lattice constant was however fixed at a = 255 nm.

After completing the fabrication of the passive Si_3N_4 PC backbone, highly luminescent red-emitting CQDs were spin-coated and dried. In particular, we employed core-shell-shell CdSe/CdS/ZnS CQDs,[37] whose schematic structure and transmission electron microscope image are shown in Fig. 1. From separate spectroscopic ellipsometry measurements, we estimated the index of refraction of the spin-coated CQD layer to be n ~ 1.75 at the CQD emission peak λ ~ 615 nm. Spin-coating of CQDs is a great advantage in terms of simple and facile preparation of optical gain medium.[38, 39] Ideal spin-coating process would result in CQDs filling the air-holes selectively without leaving any residue on top of the PC slab, which would then ensure lasing action only at the LIB band-edge modes. In a real-world application, however, a CQD over-layer is inevitably formed on the entire PC backbone structure after the spin-coating process, which is schematically depicted in Fig. 1 and also taken into account in our model calculations. The existence of the CQD over-layer infers that lasing action may occur not only at the LIB band-edge modes but also at the HIB band-edge modes. We note that the M-point band-gap is narrow (~12 nm) so that all the M-point band-edge modes can be designed to fall within the CQD emission bandwidth (~34 nm in FWHM). We intentionally generated a couple of scratches into the CQD over-layer to uncover the underlying Si_3N_4 PC slab. Shown in Fig. 3e is an SEM image of a CQD-coated sample with the scratch marks. Figure 3f is an amplified SEM image of the scratched portion, where some of the air-holes become visible. One can clearly see from the figure that the air-holes are completely filled with the CQDs with no sign of air void.

We conducted micro-photoluminescence experiment—in ambient atmosphere and at room-temperature—in order to collect emission spectra from the fabricated CQD-PC laser samples. Fabricated devices were optically pumped using a frequency-doubled (532 nm) Nd:YAG laser in a pulsed mode (pulse duration 400 ps; repetition rate 1 kHz). A 10× objective lens (NA = 0.31), oriented at 45° to the surface normal, was used to excite an individual PC pattern, while emission signal was collected from the surface normal direction. The focusing lens was intentionally off-focused such that pump spot size became about 60 μm × 80 μm on

the sample surface, somewhat elongated due to the oblique incidence but still large enough to cover an individual PC pattern (50 μm × 50 μm). We examined two kinds of samples with different CQD over-layer thicknesses, which were prepared conveniently by controlling
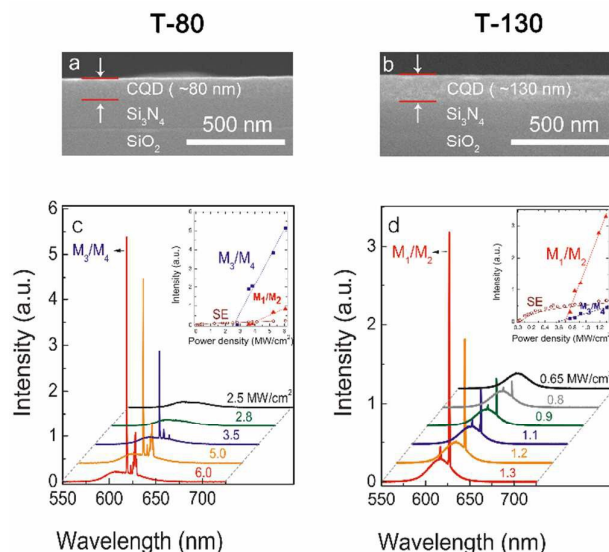
Fig. 4 Lasing properties of CQD-PC band-edge lasers. (a)(b) Cross-sectional SEM images of two CQD-PC devices with different CQD layer thicknesses: (a) T-80 and (b) T-130, from which the CQD over-layer thicknesses were measured to be ~ 80 nm and ~ 130 nm, respectively. The SEM images were taken from planar part of samples for thickness characterization. (c)(d) Photoluminescence spectra measured from the CQD-PC band-edge laser devices at various pump power density levels: (c) T-80 and (d) T-130. The insets are light-in versus light-out (L-L) curves drawn from the measured spectra; each inset includes the L-L curves for the HIB (red, solid triangles) and LIB (blue, solid squares) band-edge modes as well as spontaneous emission (brown, open circles).

CQD concentration in cyclohexane solution. Figures 4a and 4b show cross-sectional SEM images of those two kinds of samples, from which the thicknesses of the CQD over-layer on top of the Si_3N_4 backbone slab are directly determined to be $t_{CQD} \approx$ 80 nm and 130 nm; we name them T-80 and T-130 hereafter. Figures 4c and 4d show emission spectra from the two samples, recorded at various pump power levels. Above thresholds, two major sharp laser lines appeared for the both of T-80 and T-130. The spectral separation $\Delta\lambda$ between the two lasing modes is measured to be ~11 nm, which is close to the simulated M-point band-gap of ~12 nm—Fig. 2c. We therefore identify the two major laser lines as the two band-edge mode groups on both sides of the M-point band-gap: M_1/M_2 for the long wavelength laser line and M_3/M_4 for the short wavelength laser line. Exact mode identification between M_1 and M_2, however, requires further detailed investigation and is beyond the scope of the present study, while M_3 and M_4 are degenerate modes as mentioned previously.

We also note in Figs. 4c and 4d that the dominant lasing mode is switched between T-80 and T-130, which we believe supports our mode identification. First, let us imagine that the CQD over-layer thickness is zero so that CQDs fill the air-holes only. Then it is highly unlikely that a HIB band-edge mode (M_1 or M_2) lase because the modal overlap with optical gain is negligible, which leaves a LIB

band-edge mode (M_3 or M_4) for the only possible lasing mode. If a thin CQD over-layer is assumed to be added, however, it is easy to imagine that the both groups of band-edge modes can lase with the dominance of the LIB band-edge mode, which we believe is the case with T-80. Meanwhile, a small amount of available optical gain (due to a relatively thin CQD over-layer) makes the laser threshold high, ~ 2.5 MW/cm^2 (or ~ 1000 μJ/cm^2), as shown in the inset of Fig. 4c. If the CQD over-layer becomes fairly thick (*i.e.*, comparable to or thicker than the air-hole depth) as for T-130, however, optical gain available should become higher and at the same time spatially more homogeneous so that the both groups of band-edge modes can lase at relatively low thresholds. On the other hand, the HIB band-edge modes (M_1 or M_2), whose Q-factors are slightly higher, are likely to lase first, take most of the available gain, and thus become dominant; Q-factors estimated from computer simulations on the corresponding "cold" (*i.e.*, population-inverted, and therefore optically transparent) PC structure are ~1,800 and ~1,600 for the HIB and LIB band-edge modes, respectively. Figure 4d confirms that laser emission intensity of the HIB band-edge mode is indeed much stronger than that of the LIB band-edge mode. The inset of Fig. 4d indicates that laser thresholds are now significantly reduced to ~0.7 MW/cm^2 (or ~300 μJ/cm^2), which is a reduction by a factor of ~4 when compared with those of T-80, consistent with our prediction. We note that this kind of threshold pulse energy density is in the same order of magnitude as those of CQD VCSELs[17] and DFB lasers[19] demonstrated earlier, despite the much smaller CQD gain volume.

It should be worth to mention that the strength of spontaneous emission in Figs. 4c and 4d is exaggerated relative to the laser intensities because spontaneous emission is isotropic in its emission direction so that its detection efficiency in the surface-normal direction is far better than for the M-point band-edge modes whose propagation directions are along the wafer plane. While the M-point band-edge mode naturally fits the lateral mode coupling condition and is therefore compatible with on-chip integration of photonic devices, a Γ-point band-edge mode could be employed for surface-normal laser emission,[32-34] if needed. We also note in Fig. 4c that some complex laser modes appear in addition to the two major laser lines, which we attribute to the Fabry-Perot oscillation modes developed across the entire PC pattern as a result of high levels of optical excitation. In addition, we did not notice any significant change in our photoluminescence spectra up to a few minutes in total accumulated data collection time, except for a slight decrease in emission intensity by less than 10%. We attribute such a stable laser operation to the high quality material passivation enabled by the core-shell-shell CQD structure.

In conclusion, we successfully demonstrated the room-temperature lasing operation of a novel CQD-PC band-edge laser. Core-shell-shell type CdSe/CdS/ZnS CQDs were simply spin-coated as gain material on a passive 2D square lattice PC backbone slab composed of Si_3N_4. Fabricated CQD-PC devices lased at both of the HIB and LIB band-edge modes at M-point, as designed. The modal dominance among them was found to be dependent on the thickness of CQD over-layer, offering a convenient way how to control the lasing mode. We expect that further optimizations in structural design and device fabrication will improve laser performance and

mode controllability. Unlike conventional PC lasers built on an epitaxial MQW structure, our CQD-PC lasers can be made cheap. In addition, optical gain (or CQDs) is applied extrinsically onto a pre-made passive PC backbone, which implies that spatial locations and sizes of lasers can be tailored, making the proposed device and fabrication schemes suitable and attractive for the future high density photonic integrated circuits where many active and passive photonic components are to be integrated on a single chip platform.

Experimental

FDTD Simulation

Numerical simulations were performed by employing a commercial FDTD software package (FDTD Solutions, Lumerical Solutions) to generate photonic band structure of the 2D square lattice CQD-PC and E-field profiles of the associated band-edge modes. The Bloch boundary conditions in the x- and y-directions are applied, while perfect matching layers on the top and bottom boundaries of the simulation unit cell is used in the z-direction. Multiple random electric dipole sources are launched to excite the unit cell. The information on the complex index of refraction of CQDs, which was used in the FDTD simulations, was obtained from spectroscopic ellipsometry measurement on a separately prepared thin CQD film.

Fabrication of Passive PC

For fabrication of the passive 2D PC backbone, layers of SiO_2 and Si_3N_4 were sequentially deposited on Si substrate using PECVD, where the SiO_2 layer serves the bottom cladding of the Si_3N_4 waveguide layer. A positive electron-beam resist (ZEP520A) was spun on the Si_3N_4 surface at 4,000 rpm for 40 s to obtain a 200-nm-thick resist layer, which was then baked at 190°C for 2 min, and thereafter subjected to electron beam exposure to generate a 2D square lattice PC pattern in an electron beam lithography system (JEOL JBX-6300FS at 100 keV acceleration voltage and 1 nA current). After developing the exposed resist using ZED-N50 for 5 min, a square lattice 2D hole array was defined on the resist film. The resist pattern was transferred to the underlying Si_3N_4 layer using CF_4-based RIE ($CF_4 : O_2 = 40 : 2$ in sccm, 100 W RF power, 42 mTorr) for 1 min 40 sec. The e-beam resist was removed by dipping the sample in piranha solution for 3 min. For multiple purposes (easy identification of individual PC pattern, and scattering of laser light off from device surface, *etc.*), a mesh grid was constructed onto the fabricated Si_3N_4 PC backbone structure by conventional photolithography. RIE etching of the mesh grid pattern and subsequent photoresist removal were performed as before, which completes the PC backbone fabrication process. We intentionally rotated the square lattice 2D PC pattern by 45° with respect to the mesh grid so that the light emitting from the M-point band-edge modes be scattered out in the in-plane directions along the mesh grid.

CQD Synthesis and Film Deposition

Core-shell-shell CQDs of CdSe/CdS/ZnS were synthesized based on the previous publications. The wavelengths of the first excitation absorption and maximum photoluminescence were measured to be 584 nm and 615 nm, respectively. The FWHM spontaneous emission linewidth was ~34 nm. To make a film with thickness of 80

nm, CQDs dispersed in cyclohexane solution as 2.1 wt% were spin-coated at 1000 rpm. To increase the thickness of CQDs to 130 nm, the concentration of CQDs in cyclohexane was increased to 2.7 wt%, and spin-coated at 1000 rpm. The cyclohexane solution was evaporated quickly during spin-coating to form a uniform film composed only of the CQDs.

Optical Measurement

Micro-photoluminescence measurements were performed to excite the CQD-PC laser device and to acquire emission signal from it. Pump laser beam from a 532 nm, frequency-doubled, pico-second pulsed Nd:YAG laser with 1 kHz repetition rate was focused down by a 10× objective lens (NA = 0.31) to an elliptical spot (~80 μm × ~60 μm) due to 45°-angled incidence, which is large enough to cover an individual PC pattern. Light emitted from the laser device was fed to a spectrometer (DW700, Dongwoo Optron) for spectral analyses

Acknowledgements

References

1. O. Painter, R. K. Lee, A. Scherer, A. Yariv, J. D. O'Brien, P. D. Dapkus and I. Kim, *Science*, 1999, **284**, 1819.
2. R. F. Oulton, V. J. Sorger, T. Zentgraf, R. M. Ma, C. Gladden, L. Dai, G. Bartal and X. Zhang, *Nature*, 2009, **461**, 629.
3. M. A. Noginov, G. Zhu, A. M. Belgrave, R. Bakker, V. M. Shalaev, E. E. Narimanov, S. Stout, E. Herz, T. Suteewong and U. Wiesner, *Nature*, 2009, **460**, 1110.
4. R. M. Ma, R. F. Oulton, V. J. Sorger, G. Bartal and X. A. Zhang, *Nat. Mater.*, 2011, **10**, 110.
5. W. Zhou, M. Dridi, J. Y. Suh, C. H. Kim, D. T. Co, M. R. Wasielewski, G. C. Schatz and T. W. Odom, *Nat. Nanotechnol.*, 2013, **8**, 506.
6. D. Ohnishi, T. Okano, M. Imada and S. Noda, *Opt. Express*, 2004, **12**, 1562.
7. M. Nomura, S. Iwamoto, K. Watanabe, N. Kumagai, Y. Nakata, S. Ishida and Y. Arakawa, *Opt. Express*, 2006, **14**, 6308.
8. K. Nozaki, S. Kita and T. Baba, *Opt. Express*, 2007, **15**, 7506.
9. S. Kim, J. Lee and H. Jeon, *Opt. Express*, 2010, **19**, 1.
10. S. Kim, S. Kim, K. Hwang, H. Jeon and H. J. Kim, *Appl. Phys. Express*, 2011, **4**, 122101.
11. H. G. Park, S. H. Kim, S. H. Kwon, Y. G. Ju, J. K. Yang, J. H. Baek, S. B. Kim and Y. H. Lee, *Science*, 2004, **305**, 1444.
12. R. Rossetti, S. Nakahara and L. E. Brus, *J. Chem. Phys.*, 1983, **79**, 1086.
13. C. B. Murray, D. J. Norris and M. G. Bawendi, *J. Am. Chem. Soc.*, 1993, **115**, 8706.
14. M. A. Hines and P. Guyot-Sionnest, *J. Phys. Chem.-Us*, 1996, **100**, 468.
15. B. O. Dabbousi, J. RodriguezViejo, F. V. Mikulec, J. R. Heine, H. Mattoussi, R. Ober, K. F. Jensen and M. G. Bawendi, *J. Phys. Chem. B*, 1997, **101**, 9463.
16. C. B. Murray, C. R. Kagan and M. G. Bawendi, *Annu. Rev. Mater. Sci.*, 2000, **30**, 545.
17. C. Dang, J. Lee, C. Breen, J. S. Steckel, S. Coe-Sullivan and A. Nurmikko, *Nat. Nanotechnol*, 2012, **7**, 335.
18. B. Guzelturk, Y. Kelestemur, K. Gungor, A. Yeltik, M. Z. Akgul, Y. Wang, R. Chen, C. Dang, H. D. Sun and H. V. Demir, *Adv. Mater.*, 2015, **27**, 2741.
19. K. Roh, C. Dang, J. Lee, S. T. Chen, J. S. Steckel, S. Coe-Sullivan and A. Nurmikko, *Opt. Express*, 2014, **22**, 18800.
20. P. Lodahl, A. F. van Driel, I. S. Nikolaev, A. Irman, K. Overgaag, D. Vanmaekelbergh and W. L. Vos, *Nature*, 2004, **430**, 654.
21. N. Ganesh, W. Zhang, P. C. Mathias, E. Chow, J. A. N. T. Soares, V. Malyarchuk, A. D. Smith and B. T. Cunningham, *Nat. Nanotechnol.*, 2007, **2**, 515.
22. L. Martiradonna, L. Carbone, A. Tandaechanurat, M. Kitamura, S. Iwamoto, L. Manna, M. De Vittorio, R. Cingolani and Y. Arakawa, *Nano Lett.*, 2008, **8**, 260.
23. A. Qualtieri, F. Pisanello, M. Grande, T. Stomeo, L. Martiradonna, G. Epifani, A. Fiore, A. Passaseo and M. De Vittorio, *Microelectron Eng*, 2009, **87**, 1435.
24. S. Shukla, R. Kumar, A. Baev, A. S. L. Gomes and P. N. Prasad, *J. Phys. Chem. Lett.*, 2010, **1**, 1437.
25. S. Gupta and E. Waks, *Opt. Express*, 2013, **21**, 29612.
26. F. S. Diana, A. David, I. Meinel, R. Sharma, C. Weisbuch, S. Nakamura and P. M. Petroff, *Nano Lett.*, 2006, **6**, 1116.
27. F. Pisanello, L. Martiradonna, A. Qualtieri, T. Stomeo, M. Grande, P. P. Pompa, R. Cingolani, A. Bramati and M. De Vittorio, *Photonic Nanostruct.*, 2011, **10**, 319.
28. X. S. Xu and H. Y. Wang, *Nanoscale*, 2016, **8**, 342.
29. S. H. Kwon, H. Y. Ryu, G. H. Kim, Y. H. Lee and S. B. Kim, *Appl. Phys. Lett.*, 2003, **83**, 3870.
30. S. H. Kwon, S. H. Kim, S. K. Kim and Y. H. Lee, *Opt. Express*, 2004, **12**, 5356.
31. C. O. Cho, J. Jeong, J. Lee, H. Jeon, I. Kim, D. H. Jang, Y. S. Park and J. C. Woo, *Appl. Phys. Lett.*, 2005, **87**, 161102.
32. Y. Park, S. Kim, C. Moon, H. Jeon and H. J. Kim, *Appl. Phys. Lett.*, 2007, **90**, 171115.
33. D. U. Kim, S. Kim, J. Lee, S. R. Jeon and H. Jeon, *IEEE Photon. Technol. Lett.*, 2011, **23**, 1454.
34. S. Ahn, H. Kim, H. Jeon, J. R. Oh, Y. R. Do and H. J. Kim, *Appl. Phys. Express*, 2012, **5**, 042102.
35. S. Kim, S. Ahn, K. Min, S. Kim, H. Jeon, P. Regreny and C. Seassal, *Appl. Phys. Express*, 2013, **6**, 042703.
36. K. Min, S. Choi, Y. Choi and H. Jeon, *Nanoscale*, 2014, **6**, 14531.
37. J. Lim, S. Jun, E. Jang, H. Baik, H. Kim and J. Cho, *Adv. Mater.*, 2007, **19**, 1927.
38. S. Coe, W. K. Woo, M. Bawendi and V. Bulovic, *Nature*, 2002, **420**, 800.

Nanoscale Accepted Manuscript

39.   K. S. Cho, E. K. Lee, W. J. Joo, E. Jang, T. H. Kim, S. J.
       Lee, S. J. Kwon, J. Y. Han, B. K. Kim, B. L. Choi and J.
       M. Kim, *Nat. Photonics*, 2009, **3**, 341.